

Regression of Melanoma Following Intravenous Injection of Plumbagin Entrapped in Transferrin-Conjugated, Lipid-Polymer Hybrid Nanoparticles

This article was published in the following Dove Press journal:
International Journal of Nanomedicine

Intouch Sakpakdeejaroen¹
Sukrut Somani¹
Partha Laskar¹
Margaret Mullin²
Christine Dufès¹ 

¹Strathclyde Institute of Pharmacy and Biomedical Sciences, University of Strathclyde, Glasgow, G4 0RE, UK;

²College of Medical, Veterinary and Life Sciences, University of Glasgow, Glasgow, G12 8QQ, UK

Background: Plumbagin, a naphthoquinone extracted from the officinal leadwort presenting promising anti-cancer properties, has its therapeutic potential limited by its inability to reach tumors in a specific way at a therapeutic concentration following systemic injection. The purpose of this study is to assess whether a novel tumor-targeted, lipid-polymer hybrid nanoparticle formulation of plumbagin would suppress the growth of B16-F10 melanoma *in vitro* and *in vivo*.

Methods: Novel lipid-polymer hybrid nanoparticles entrapping plumbagin and conjugated with transferrin, whose receptors are present in abundance on many cancer cells, have been developed. Their cellular uptake, anti-proliferative and apoptosis efficacy were assessed on various cancer cell lines *in vitro*. Their therapeutic efficacy was evaluated *in vivo* after tail vein injection to mice bearing B16-F10 melanoma tumors.

Results: The transferrin-bearing lipid-polymer hybrid nanoparticles loaded with plumbagin resulted in the disappearance of 40% of B16-F10 tumors and regression of 10% of the tumors following intravenous administration. They were well tolerated by the mice.

Conclusion: These therapeutic effects, therefore, make transferrin-bearing lipid-polymer hybrid nanoparticles entrapping plumbagin a highly promising anti-cancer nanomedicine.

Keywords: plumbagin, transferrin, tumor targeting, lipid-polymer hybrid nanoparticles, cancer therapy

Introduction

Plumbagin (5-hydroxy-2-methyl-naphthalene-1,4-dione), a naphthoquinone extracted from the roots of the *Plumbago indica* plant (known as officinal leadwort and widely used in traditional Chinese medicine),¹ has recently attracted considerable interest due to its chemopreventive and therapeutic efficacy against many types of cancer, including breast,² ovarian,³ lung,⁴ prostate⁵ and melanoma.⁶ Its anti-cancer effect was shown to occur through a wide range of mechanisms, such as the generation of reactive oxygen species, the decrease in intracellular glutathione levels and the activation of p53. Plumbagin also inhibits the nuclear factor-κB (NF-κB), the signal transducer and activator of transcription 3 (STAT3), the p38 mitogen-activated protein kinase (MAPK) and the phosphoinositide 3-kinase (PI3K)/the protein kinase B/Akt (PKB/AKT)/the mammalian target of rapamycin (mTOR) signaling molecules, c-Jun N-terminal kinase, resulting in potentiation of apoptosis.^{4,7–11}

Correspondence: Christine Dufès
Strathclyde Institute of Pharmacy and Biomedical Sciences, University of Strathclyde, Glasgow G4 0RE, United Kingdom
Tel +44 1415483796
Fax +44 1415522562
Email C.Dufes@strath.ac.uk

The therapeutic use of plumbagin has however been hampered so far, due to its high lipophilicity (log P 3.04),¹² limited solubility in water (79 µg/mL)¹² and lack of stability, which limited its biopharmaceutical applications. Furthermore, this drug failed to specifically reach tumors at a therapeutic concentration and was rapidly eliminated, with a short biological half-life of 35.89 ± 7.95 min.¹³

This drawback could be overcome by loading the drug within delivery systems able to entrap this lipophilic drug, enhance its water solubility and its circulation time and release it in a sustained way, thus lowering the frequency of administration and the occurrence of secondary effects of the drug.

Several lipid-based vesicles (thermosensitive and polyethylene glycol (PEG)-modified liposomes)^{13,14} and polymer-based nanoparticles (poly(lactic-co-glycolic acid) (PLGA) microspheres and PLGA-PEG nanoparticles)^{15,16} have previously been investigated to enhance the therapeutic potential of plumbagin, but with limited effects on the anti-cancer efficacy of plumbagin so far.

We now would like to develop novel lipid-polymer hybrid nanoparticles combining distinct characteristics of PEGylated liposomes and polymeric nanoparticles: (i) an hydrophobic polymer core that is biocompatible, biodegradable and capable of carrying the poorly water-soluble plumbagin and controlling its release; (ii) a lipid layer that can reduce water penetration rate into the nanoparticles, while at the same time preventing the entrapped drug from freely diffusing out of the nanoparticles; (iii) an hydrophilic PEG shell that can prevent a rapid clearance of the delivery system by mononuclear phagocytic system, improving the blood circulation half-life of the drug.¹⁷ Furthermore, as iron is essential for the growth of cancer cells and can be carried to tumors by transferrin (Tf), whose receptors are overexpressed on many cancer cell lines,^{18–23} we hypothesize that conjugating lipid-polymer hybrid nanoparticles with transferrin would increase the delivery of plumbagin by active targeting to the cancer cells, thus leading to its enhanced therapeutic efficacy. The combination of transferrin with the passive accumulation of lipid-polymer hybrid nanoparticles in tumors as a result of the enhanced permeability and retention (EPR) effect²⁴ is expected to provide tumor-selective targeting of the lipid-polymer hybrid nanoparticles to the cancer cells.

The objectives of this study were therefore 1) to develop and characterize plumbagin-entrapping lipid-polymer hybrid

nanoparticles conjugated with transferrin, 2) to evaluate their uptake, anti-proliferative and apoptosis efficacy on various cancer cell lines in vitro and 3) to assess their therapeutic efficacy in vivo, following systemic administration to tumor-bearing mice.

Materials and Methods

Cell Lines and Reagents

Plumbagin (5-hydroxy-2-methyl-1,4-naphthoquinone, from *Plumbago indica*), hydrogenated phosphatidylcholine (HPC), human holo-transferrin (Tf), Resomer[®] RG 503 H (acid-terminated poly(lactide-co-glycolide) (PLGA-COOH), lactide: glycolide 50:50, viscosity 0.32–0.44 dL/g, MW 24 000–38 000 Da) and all other chemicals not specifically mentioned below were purchased from Sigma Aldrich (Poole, UK). 1,2-distearoyl-sn-glycero-3-phosphoethanolamine-N-[maleimide (polyethylene glycol)-2000] (DSPE-PEG2K-MAL) came from Jenkem Technology (Plano, TX). Dulbecco's Modified Eagle Medium (DMEM) and Roswell Park Memorial Institute 1640 (RPMI-1640) cell culture media, fetal bovine serum (FBS), L-glutamine and penicillin-streptomycin were purchased from Invitrogen (Paisley, UK). A431 human epidermoid carcinoma and T98G glioblastoma were obtained from the European Collection of Cell Cultures (Salisbury, UK), while Bioware[®] B16-F10-luc-G5 mouse melanoma expressing the firefly luciferase was purchased from Caliper Life Sciences (Hopkinton, MA). BD Pharmingen[®] Fluorescein isothiocyanate (FITC) Annexin V Apoptosis Detection Kit I was obtained from BD Biosciences (San Jose, CA).

Preparation and Optimization of Lipid–Polymer Hybrid Nanoparticles Entrapping Plumbagin

Lipid–polymer hybrid nanoparticles (LPN) entrapping plumbagin were prepared by shaking a mixture of hydrogenated phosphatidylcholine (2 mg) and DSPE-PEG2K-MAL (3 mg) at molar ratios of 70:30, in 5 mL deionized water at 65°C for 1 h. PLGA-COOH (25 mg) and plumbagin (2.5 mg) in acetone (2.5 mL) were then added dropwise under moderate stirring. The mixture was stirred overnight at 25°C to evaporate all the organic solvent. The nanoparticles were then collected by centrifugation at 7 500 rpm (6 600 g) at 20°C for 30 min (Hermle[®] Z323K centrifuge, Wehingen, Germany), using Vivaspin[®] 20 centrifuge tubes (molecular weight cut-off: 100 000 Daltons)

(Sartorius Ltd., Epsom, UK). They were washed twice with deionized water (2 mL) to remove excess plumbagin, before being re-suspended in deionized water (1 mL) and stored at 4°C.

The nanoparticles were optimized by varying two factors: (1) the weight ratio of lipid (HPC and DSPE-PEG2K-MAL) to PLGA-COOH polymer (1:10, 2:10, 4:10, 6:10, 8:10 and 10:10) and (2) the molar ratio of HPC to DSPE-PEG2K-MAL (90:10, 85:15, 80:20, 70:30, 60:40 and 50:50), while fixing the theoretical drug loading at 10% of polymer weight, the concentration of polymer in organic solvent at 10 mg/mL and the volume ratio of water to organic solvent at 2:1.

To determine the entrapment efficiency of plumbagin, the nanoparticles (10 µL) were disrupted with isopropanol (990 µL), followed by centrifugation at 10 000 rpm (9 300 g) for 10 min with an IEC Micromax[®] centrifuge (ThermoFisher Scientific, Waltham, MA). The amount of plumbagin in the supernatant was determined by spectrophotometry (λ_{max} : 420 nm), by using an Agilent Varian Cary[®] 50 UV-Vis spectrophotometer (Agilent Technologies, Santa Clara, CA). The results were expressed as percentage entrapment efficiency.

Preparation of Transferrin-Bearing Lipid–Polymer Hybrid Nanoparticles Entrapping Plumbagin

Tf was conjugated to the LPN using the thiol–maleimide “click” reaction. To do so, Tf (10 mg) dissolved in sodium phosphate buffer (50 mM) containing sodium chloride (150 mM) (pH 8, 1 mL), was thiolated following incubation with 10-fold molar excess of 2-iminothiolane (85 µL of Traut’s reagent, 2 mg/mL in distilled water) at 25°C for 2 h whilst stirring. The thiolated Tf was then separated from unreacted Traut’s reagent by centrifugation at 9 500 rpm (10 500 g) at 20°C for 15 min (Hermle[®] Z323K centrifuge, Wehingen, Germany), with Vivaspin[®] 6 centrifuge tubes (molecular weight cut-off: 5 000 Daltons) (Sartorius Ltd., Epsom, UK). It was immediately conjugated to the LPN and incubated for 2 h at 25°C whilst stirring. Unreacted Tf was then removed from the resulting LPN by centrifugation at 7 500 rpm (6 600 g) at 20°C for 15 min, with Vivaspin[®] 6 centrifuge tubes (molecular weight cut-off: 100 000 Daltons) (Sartorius Ltd., Epsom, UK).

The formation of LPN was visualized by transmission electron microscopy (TEM). Briefly, Formvar/Carbon-

coated copper grids (400 mesh) were glow discharged. Each sample (3 µL) was then dropped onto the hydrophilic support film. Dried samples were imaged using the JEOL 1200 transmission electron microscope (JEOL USA, Inc., Peabody, MA) operating at 80 kV fitted with a Gatan 794 MultiScan[®] camera (Gatan, Pleasanton, CA).

The amount of Tf conjugated to the LPN was determined by Lowry assay,²⁵ using a previously reported method.²⁶

The hydrodynamic size and zeta potential of LPN were measured by photon correlation spectroscopy and laser Doppler electrophoresis, with a Zetasizer Nano-ZS[®] (Malvern Instruments, Malvern, UK).

Plumbagin Release from the Transferrin-Bearing Lipid–Polymer Hybrid Nanoparticles

The release of plumbagin was studied using a dialysis method at pHs 7.4 and 5.5, respectively mimicking the physiological pH in normal tissues and blood, and the extracellular microenvironment of tumor tissues. To do so, plumbagin (500 µg/mL in phosphate buffer for 1 mL) either formulated as Tf-bearing LPN, control LPN or in solution, was transferred into a SnakeSkin[®] dialysis bag (molecular weight cut-off: 3 500 Daltons) (ThermoFisher Scientific, Waltham, MA) and was dialyzed against 50 mL of phosphate buffer pHs 7.4 and 5.5. The samples were kept at 37°C with continuous stirring (100 rpm). At specific time intervals (30 min, then every hour for the first 6 h (1 h, 2 h, 3 h, 4 h, 5 h, 6 h), then every 2 h for the next 6 h (8 h, 10 h, 12 h), and 24 h), 1 mL of the dialysate was withdrawn in triplicates and then replaced with an equal volume of fresh buffer. The amount of plumbagin in the sample was determined by spectrophotometry (Agilent Technologies, Santa Clara, CA) and reported as a percentage cumulative drug release.

Cell Culture

B16-F10-luc-G5 melanoma cell line was grown in RPMI-1640 medium, while A431 human epidermoid carcinoma and T98G glioblastoma cell lines were grown in DMEM medium. Both media were supplemented with 10% (v/v) fetal bovine serum, 1% (v/v) L-glutamine and 0.5% (v/v) penicillin-streptomycin. Cells were cultured at 37°C in a humid atmosphere of 5% CO₂.

Cellular Uptake

To investigate the intracellular accumulation of plumbagin, cells were seeded at a density of 2×10^5 cells/well in 6-well plates. After 72 h, they were treated with plumbagin (10 $\mu\text{g}/\text{well}$), either formulated as Tf-bearing LPN, control LPN, or in solution (prepared from a stock plumbagin solution of 100 mg/mL in DMSO), for 3 h. Following incubation with the treatments, they were harvested and washed twice with cold phosphate buffer saline (PBS) (3 mL) to remove the nanoparticles that were not taken up or bound to the cell surface. Cells were then lysed with Triton-X (5%, 1 mL) and incubated at 37°C for 24 h before being centrifuged at 10 000 rpm (9 300 g) for 15 min with an IEC Micromax[®] centrifuge (ThermoFisher Scientific, Waltham, MA). The amount of plumbagin in the surfactant was determined by spectrophotometry (λ_{max} : 420 nm), using a FlexStation 3[®] multi-mode microplate reader (Molecular Devices, Sunnyvale, CA).

To further confirm the cellular uptake of LPN, plumbagin was replaced with coumarin-6, a fluorescent lipophilic drug model ([Supplementary Table 1, supplementary information](#)). Tf-bearing and control LPN entrapping coumarin-6 were prepared and characterized using the same protocol as described above. They were used for determining the cellular uptake of coumarin-6 in B16-F10-luc-G5 cells.

Confocal microscopy was used for qualitative analysis of the LPN uptake by the cells. In brief, B16-F10-luc-G5 cells were seeded in 6-well plates containing a glass cover slip, at a density of 1×10^5 cells/well. They were grown for 24 h before being treated with coumarin-6 (1 $\mu\text{g}/\text{well}$), either entrapped in Tf-bearing LPN, control LPN or left in solution. Following 2-h treatment, they were washed twice with 3 mL cold PBS, followed by fixation with 2 mL formaldehyde solution (3.7% in PBS) for 10 min at 25°C. Subsequently, they were washed twice with 3 mL PBS, then incubated with 3 mL Triton-X solution (0.1%) at 25°C for 5 min, before adding 3 mL bovine serum albumin in PBS (1% w/v) followed by incubation at 37°C for 30 min to reduce the non-specific binding. The staining of the cells was done with Alexa Fluor[®] 647 dye (one unit of dye in 200 μL of PBS) incubated at 25°C for 20 min before mounting the coverslip on a glass slide with Vectashield[®] mounting medium containing 4',6-diamidino-2-phenylindole (DAPI). The confocal images were observed with a Leica TCS SP-5 confocal microscope (Wetzlar, Germany). Coumarin-6 was excited with the

505 nm laser line (emission bandwidth: 515–558 nm), while DAPI (staining the nuclei of the cells) was excited with the 405 nm laser line (emission bandwidth: 415–491 nm) and Alexa Fluor[®] 647 (staining the cell cytoplasm) was excited with the 633 nm laser line (emission bandwidth: 645–710 nm).

Flow cytometry was also used to quantify the fluorescence intensity of coumarin-6 taken up by the cancer cells. To do so, B16-F10-luc-G5 cells were seeded (1×10^5 cells/well) and grown for 24 h before treatment with coumarin-6 (50 ng/well), which was either entrapped in Tf-bearing LPN, control LPN or in solution. After 2-h treatment, they were washed twice with 3 mL cold PBS and harvested with 250 μL TrypLE[®] Express. Subsequently, 500 μL RPMI-1640 medium was added to the cell suspension. The mean fluorescence intensity (MFI) of coumarin-6 taken up by the cells was measured by flow cytometry, with a FACSCanto[®] flow cytometer (BD Biosciences, San Jose, CA) using a FITC filter (Exc_{max} : 494 nm/ Em_{max} : 520nm). Ten thousand cells (gated events) were counted for each sample.

Mechanism of Cellular Uptake

To investigate the endocytosis pathway involved in the cellular uptake of LPN, B16-F10-luc-G5 cells were seeded at a density of 2×10^5 cells/well in 6-well plates and incubated for 24 h. Cells were then pre-incubated at 37°C for 30 min with the endocytosis inhibitors transferrin (50 μM), chlorpromazine (20 $\mu\text{g}/\text{mL}$), filipin (4 $\mu\text{g}/\text{mL}$) and colchicine (40 $\mu\text{g}/\text{mL}$). The inhibitors were then removed and replaced with medium containing coumarin-6 (50 ng/mL) (entrapped in Tf-bearing LPN, control LPN or in solution) and each inhibitor at the same concentration (with the exception of chlorpromazine, which was maintained at a concentration of 5 $\mu\text{g}/\text{mL}$) for a further 2-h incubation at 37°C. The cells were then washed twice with cold PBS (3 mL) and harvested with TrypLE[®] Express (250 μL). The trypsinization reaction was then stopped by adding medium (500 μL) to the cell suspension. The mean fluorescence intensity of coumarin-6 taken up by the cells treated with LPN formulations without any inhibitor was used as a control and expressed as 100% relative cellular uptake. Ten thousand cells (gated events) were counted for each sample.

Anti-Proliferative Activity

The assessment of the anti-proliferative activity of plumbagin entrapped in LPN formulations was performed using

a 3-(4,5-dimethylthiazol-2-yl)-2,5-diphenyltetrazolium bromide (MTT) assay. All three cell lines were seeded in 96-well plates at a density of 5×10^3 cells/well for 24 h before treatment with plumbagin at various concentrations (ranging from 7.81×10^{-3} to $10 \mu\text{g/mL}$), formulated as Tf-bearing LPN, control LPN, or in solution. Following 24-h treatment, MTT solution ($50 \mu\text{L}$, 0.5% w/v in PBS) was added to each well and incubated with the cells for 4 h. The solution was then removed and DMSO ($200 \mu\text{L}$) was added to each well in order to solubilize the formazan product. The absorbance of the solution was measured at 570 nm with a Multiskan Ascent microplate reader (Thermo Labsystems, Beverly, MA). The anti-proliferative activity of the plumbagin formulations was assessed by measuring the growth inhibitory concentration for 50% of the cell population (IC_{50}) in a MTT assay. Dose–response curves were fitted to percentage absorbance values in order to obtain IC_{50} values (as the results of three independent experiments, with $n=5$ for each tested concentration).

Apoptosis Assay

Cells were seeded at a density of 2×10^5 cells per well in 6-well plates and grown for 24 h before treatment with plumbagin ($1 \mu\text{g/mL}$, corresponding to $5 \mu\text{M}$), formulated as Tf-bearing LPN, control LPN or as a solution. After 4-h incubation, the cells were harvested and centrifuged for 5 min at 2000 rpm (370 g) with an IEC Micromax[®] centrifuge (ThermoFisher Scientific, Waltham, MA) before being labeled with BD Pharmingen[®] FITC Annexin V apoptosis detection kit (BD Biosciences, San Jose, CA), following the protocol provided by the manufacturer. To do so, the cell pellets were re-suspended in $200 \mu\text{L}$ 1X Annexin V Binding Buffer (10X of the buffer containing 0.1 M HEPES/NaOH (pH 7.4), 1.4 M NaCl and 25 mM CaCl_2). Thereafter, $100 \mu\text{L}$ of cell suspension was transferred to a 5-mL culture tube, followed by $5 \mu\text{L}$ of FITC Annexin V labeling reagent and $5 \mu\text{L}$ of propidium iodide (PI). Cells were then incubated for 15 min at 20°C and protected from light. After incubation, Annexin V Binding Buffer ($400 \mu\text{L}$) was added to each tube prior to flow cytometry analysis with a FACSCanto[®] flow cytometer (BD Biosciences, San Jose, CA). Ten thousand cells (gated events) were counted for each sample. The results were reported as percentages of specific cell populations (live cells, cells in early or late apoptosis and in necrosis).

In vivo Tumoricidal Activity

The in vivo experiments were approved by the University of Strathclyde Animal Welfare and Ethical Review Body, the local ethics committee. They complied with the ARRIVE guidelines and were carried out in accordance with the United Kingdom Home Office regulations, described in the “United Kingdom Animals (Scientific Procedures) Act 1986”.

B16F10-luc-G5 cancer cells in exponential growth were subcutaneously injected to the flanks of female immunodeficient BALB/c mice (1×10^6 cells per flank). The animals were randomized into groups of five once tumors were palpable and reached a diameter of 5 mm in any direction. They were intravenously injected (2 mg/kg of body weight per injection) with plumbagin entrapped in Tf-bearing, control lipid–polymer hybrid nanoparticles or in solution (formulations diluted in glucose 5% solution), once every 2 days for 10 days. The weight of the animal was measured daily as a surrogate marker of animal welfare for the whole duration of the experiments. The tumor volume was determined by caliper measurements. The tumor width and length were measured for each tumor. Their mean was then used in the formula ($\text{volume} = d^3 \times \pi/6$). The results were expressed as relative tumor volume ($\text{rel. Volt}_x = \text{Volt}_x/\text{Volt}_0$). The responses were classified as progressive disease when the increase in relative tumor volume is higher than 1.2-fold compared with the starting tumor volume, stable disease when the relative volume is comprised between 0.7 and 1.2 of starting volume, partial response when the tumor displays a volume reduction of more than 30% (0–0.7) and complete response when the tumor has entirely disappeared, as described in the “Response Evaluation Criteria in Solid Tumors (RECIST)” guidelines.²⁷

Statistical Analysis

Results were expressed as mean \pm standard error of the mean (S.E.M) in the whole manuscript. Statistical significance of the data was determined by using one-way analysis of variance (ANOVA) and Tukey multiple comparison post-test, with Minitab[®] 17.1.0 software (Minitab Ltd., State College, PE). Differences were considered statistically significant for P values lower than 0.05.

Results

Preparation and Optimization of Lipid–Polymer Hybrid Nanoparticles Entrapping Plumbagin

The LPN were first prepared by varying the lipid to PLGA-COOH polymer weight ratio. The lipid to polymer weight ratios 1:10 and 2:10 resulted in nanoparticles having a desirable combination of particle hydrodynamic size (143.8 ± 1.0 nm and 144.4 ± 1.1 nm) and zeta potential (-57.2 ± 0.3 mV and -58.9 ± 0.8 mV) (Figure 1A). When increasing the lipid to polymer weight ratio from 4:10 to 10:10, the nanoparticles became larger (169.0 ± 0.7 nm to 183.2 ± 0.9 nm) and were more negatively charged (-63.7 ± 0.4 mV to -68.0 ± 0.8 mV). On the other hand, the entrapment efficiency of plumbagin was stable (around 40%, equivalent to 1 mg plumbagin) at all the tested

lipid to polymer weight ratios. The lipid to polymer weight ratio 2:10 was therefore chosen for further studies.

The LPN were then optimized by varying the HPC to DSPE-PEG2K-MAL molar ratio (Figure 1B). HPC to DSPE-PEG2K-MAL molar ratios 90:10, 85:15, 80:20 and 70:30 led to smaller nanoparticle hydrodynamic sizes (143.1 ± 0.6 nm to 145.8 ± 0.5 nm) and smaller zeta potentials (-57.2 ± 0.3 mV to -58.5 ± 1.4 mV), while the other ratios (60:40 and 50:50) resulted in an increase in both the particle hydrodynamic size (151.4 ± 0.6 nm to 157.0 ± 0.7 nm) and the zeta potential (-53.0 ± 0.5 mV to -53.3 ± 0.4 mV). The entrapment efficiency of plumbagin remained constant at 40–50% (equivalent to 1–1.25 mg plumbagin) when increasing the HPC to DSPE-PEG2K-MAL molar ratios.

Thus, the optimal formulation of LPN was prepared at the lipid to PLGA-COOH polymer weight ratio 2:10 and the HPC to DSPE-PEG2K-MAL molar ratio 70:30, with the concentration of polymer in organic solvent set at 10 mg/mL, plumbagin loading at 10% of polymer weight and the ratio of water to organic solvent at 2:1.

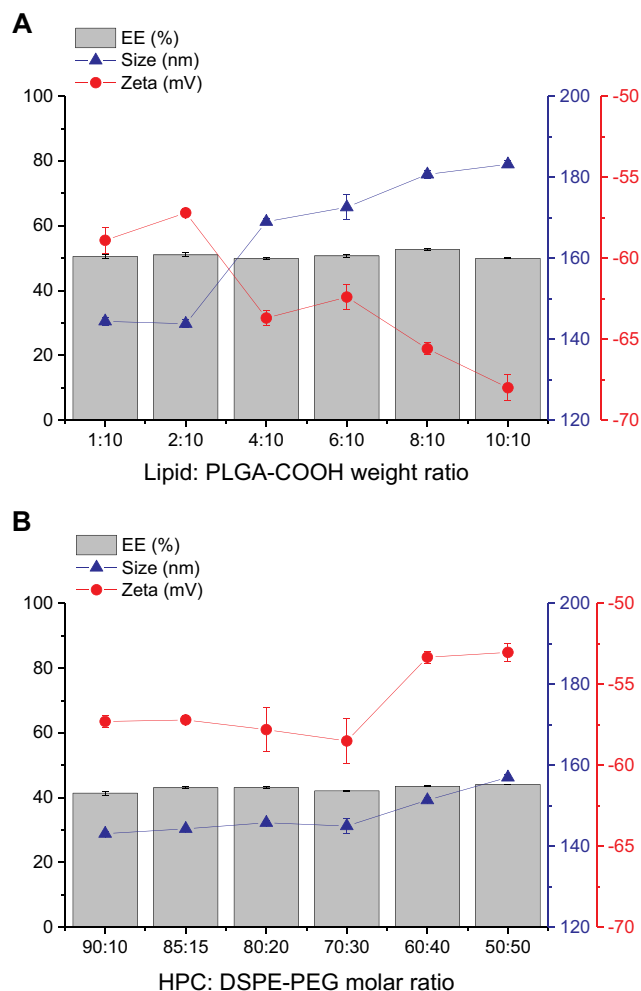


Figure 1 Optimization of lipid–polymer hybrid nanoparticles entrapping plumbagin: effects of lipid: PLGA-COOH weight ratio (A) and HSPC: DSPE-PEG2000 molar ratio (B), on particle size, zeta potential and drug entrapment efficiency (n=3).

Preparation of Transferrin-Bearing Lipid–Polymer Hybrid Nanoparticles Entrapping Plumbagin

Tf-bearing LPN entrapping plumbagin have been successfully prepared, as confirmed by TEM (Figure 2). The entrapment efficiency of plumbagin in the nanoparticles was relatively high, respectively, $46.2 \pm 1.0\%$ and $47.0 \pm 1.0\%$ for Tf-bearing and control LPN (equivalent to 1.155 ± 0.025 mg and 1.175 ± 0.025 mg of Tf, respectively). Tf was conjugated to the LPN at a level of $72.2 \pm 0.5\%$ of the initial Tf (equivalent to 7.2 ± 0.1 mg of Tf).

The grafting of Tf to the surface of the nanoparticles led to an increase in particle hydrodynamic size of Tf-bearing LPN (214.1 ± 1.5 nm, polydispersity: 0.17 ± 0.01) compared to that of control LPN (145.2 ± 0.6 nm, polydispersity: 0.16 ± 0.01). It also increased the net surface charge of Tf-bearing LPN (-46.6 ± 0.7 mV) in comparison with control LPN (-66.6 ± 0.6 mV).

Plumbagin Release from the Transferrin-Bearing Lipid–Polymer Hybrid Nanoparticles

Tf-bearing and control LPN exhibited a sustained release of the drug at pHs 7.4 and 5.5 following an initial burst release, while the drug in solution rapidly diffused through

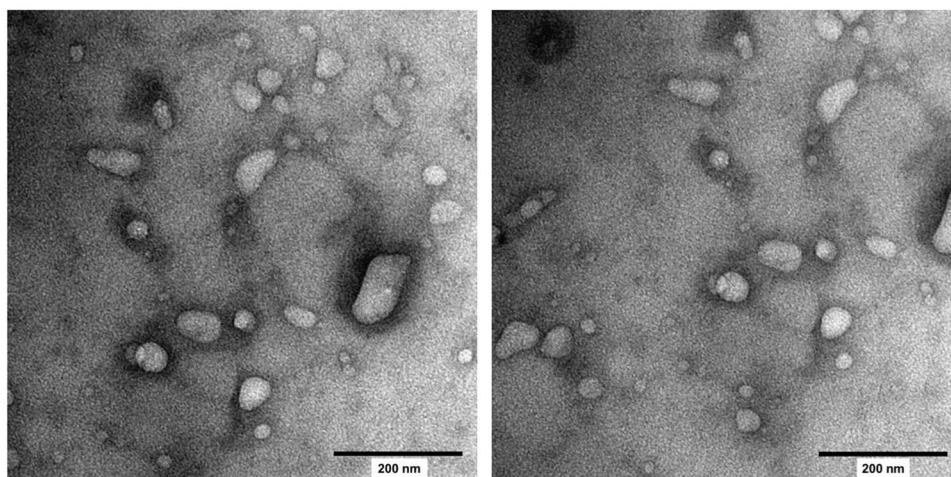


Figure 2 TEM pictures of Tf-bearing (left) and control (right) lipid-polymer hybrid nanoparticles entrapping plumbagin (Bar: 200 nm).

the dialysis membrane to be entirely released within 4 h (Figure 3). The grafting of Tf to the nanoparticles led to a lower release profile of the drug compared with control nanoparticles at both the tested pHs (respectively $81.7 \pm 1.4\%$ and $95.4 \pm 0.7\%$ at pHs 7.4 and 5.5 for Tf-bearing LPN, $90.3 \pm 1.0\%$ and $98.9 \pm 0.2\%$ at pHs 7.4 and 5.5 for control LPN over 24 h).

In vitro Biological Characterization

Cellular Uptake

The entrapment of plumbagin in Tf-bearing LPN significantly increased the uptake of plumbagin by the 3 cancer cell lines compared with control LPN and drug solution (Figure 4). In B16F10 cells, plumbagin uptake by cells treated with Tf-bearing LPN was higher than that of control LPN and drug solution, respectively by 1.6-fold and 2.1-fold ($1.44 \pm 0.06 \mu\text{g}$ for Tf-bearing LPN, $0.92 \pm 0.13 \mu\text{g}$ for control LPN and $0.70 \pm 0.17 \mu\text{g}$ for plumbagin solution). It followed a similar trend in A431 cells, with 1.3-fold and 2.7-fold enhancement following treatment with the targeted formulation compared with control nanoparticles and the drug solution ($2.46 \pm 0.04 \mu\text{g}$ for Tf-bearing LPN, $1.95 \pm 0.05 \mu\text{g}$ for control LPN and $0.92 \pm 0.07 \mu\text{g}$ for plumbagin solution). Treatment of T98G cell line with Tf-bearing LPN resulted in the highest cellular uptake of plumbagin amongst the 3 tested cell lines ($2.80 \pm 0.21 \mu\text{g}$), which was significantly higher by 1.3-fold and 2-fold than that observed after the treatment with control nanoparticles and solution ($2.24 \pm 0.13 \mu\text{g}$ for control nanoparticles and $1.43 \pm 0.05 \mu\text{g}$ for plumbagin solution).

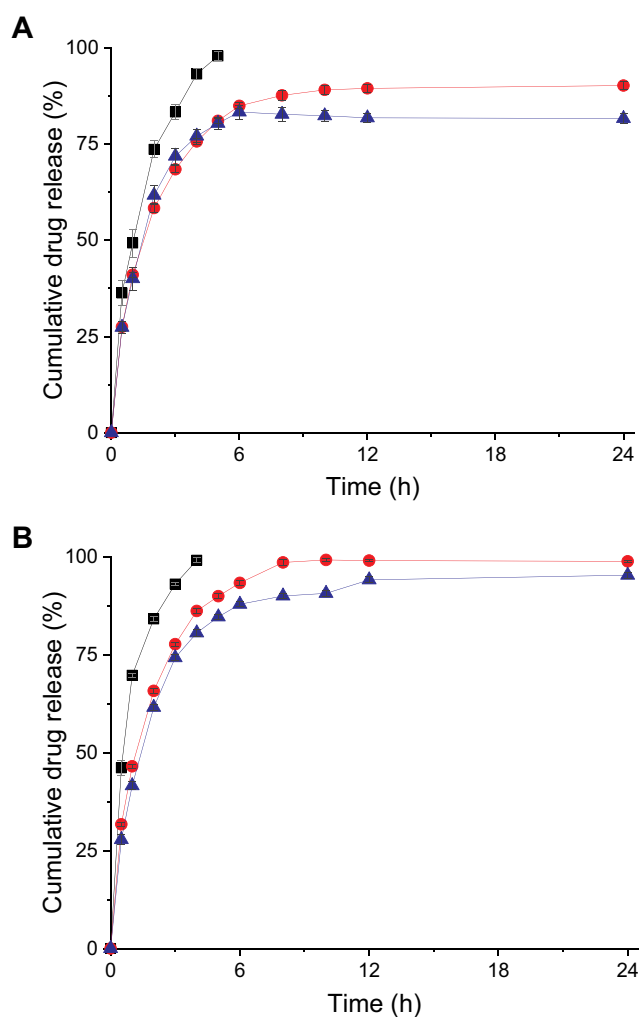


Figure 3 Drug release profile of plumbagin formulated as Tf-bearing lipid-polymer hybrid nanoparticles (\blacktriangle , blue), control lipid-polymer hybrid nanoparticles (\bullet , red) or as free drug in solution (\blacksquare , black) in phosphate buffer at pH 7.4 (A) and pH 5.5 (B) over 24 h (n=3).

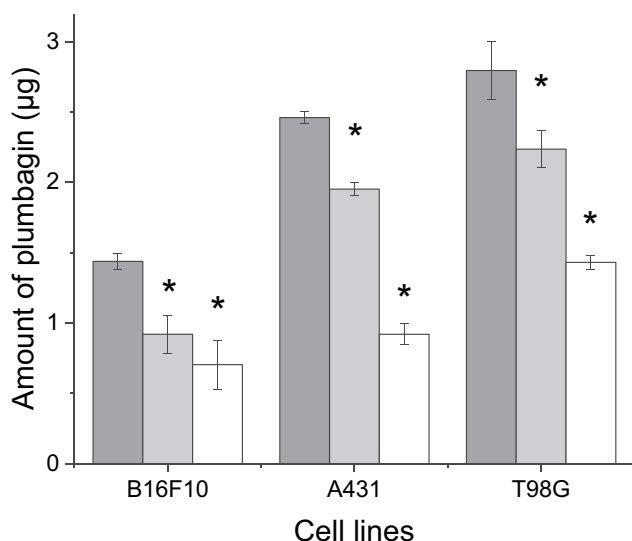


Figure 4 Cellular uptake of plumbagin (10 µg/well) formulated as Tf-bearing lipid-polymer hybrid nanoparticles (dark grey), control lipid-polymer hybrid nanoparticles (grey) or as solution (white), in B16-F10, A431 and T98G cancer cell lines (n=5) (*p<0.05 vs Tf-bearing lipid-polymer hybrid nanoparticles).

The cellular uptake of plumbagin loaded in LPN was comparable to that of coumarin-6, a lipophilic fluorescent drug model entrapped in LPN, in B16-F10 cells (Figure 5A). The grafting of Tf to the nanoparticles significantly increased the cellular uptake of coumarin-6 (mean fluorescence intensity (MFI) of 5784 ± 121 a.u.) by 1.6-fold compared to control nanoparticles (MFI of 3576 ± 123 a.u.). However, the highest uptake was observed after the treatment of the cells with coumarin-6 solution (MFI of 6567 ± 79 a.u.), which might occur by passive diffusion due to its low molecular weight (350.43 g/mol) and physicochemical properties.

These results were qualitatively confirmed by confocal microscopy (Figure 5B). The treatment of the cells with Tf-bearing LPN resulted in a higher cellular uptake of coumarin-6 compared to that observed in control nanoparticles. Cells treated with coumarin-6 solution displayed coumarin-6-derived fluorescence in their cytoplasm, which could be explained by the non-specific diffusion of the drug. Coumarin-6-derived fluorescence was disseminated in the cytoplasm of B16F10 cells following all treatments, with no visible co-localization in the nucleus.

Mechanisms of Cellular Uptake

Pre-treatment of B16-F10 cells with 50 µM of free Tf significantly decreased the uptake of coumarin-6 loaded in Tf-bearing LPN, with a relative cellular uptake of $79.8 \pm 0.9\%$ compared with that observed in the cells without pre-treatment (relative cellular uptake of 100%) (Figure 6).

Pre-treatment of the cells with chlorpromazine also resulted in a significant cellular uptake inhibition for both the targeted and control nanoparticles (respectively $79.7 \pm 3.1\%$ and $86.9 \pm 1.3\%$). The uptake of coumarin-6 loaded in Tf-bearing nanoparticles was weakly inhibited by filipin, decreasing to $92.2 \pm 3.0\%$ of that measured in cells without pre-treatment. By contrast, colchicine only caused some weak cellular uptake inhibition after treatment with control nanoparticles, with a relative cellular uptake of $93.9 \pm 3.0\%$.

Anti-Proliferative Activity

The anti-proliferative activity of plumbagin was significantly improved when formulated in LPN in comparison with the drug solution, by up to 2.5-fold (Table 1, Figure S1). It was further improved by the conjugation of Tf to these nanoparticles, by 3.2-fold in B16F10 cells, 2.8-fold in A431 cells and 3-fold in T98G cells, when compared with the drug solution. It was not possible to determine the IC₅₀ following treatment of the cells with blank LPN. Plumbagin entrapped in transferrin-bearing LPN led to the highest anti-proliferative efficacy against B16-F10 cells (IC₅₀: 0.16 ± 0.02 µg/mL), followed by A431 cells (IC₅₀: 0.63 ± 0.03 µg/mL), but only exerted a limited effect in T98G cells (IC₅₀: 2.03 ± 0.15 µg/mL).

Apoptosis Assay

Tf conjugation on plumbagin-loaded LPN significantly resulted in the highest cellular apoptosis in B16-F10 cells (Figure 7), with $89.2 \pm 0.4\%$ of the cells being apoptotic as a result of their treatment. By contrast, $80.5 \pm 0.6\%$ and $27.5 \pm 1.0\%$ of the cells were apoptotic following treatment with the control LPN or the plumbagin solution, respectively.

In A431 cells, the apoptotic effect of the targeted formulation was much lower than in B16F10 cells (total apoptosis of $20.3 \pm 1.1\%$). Control nanoparticles and plumbagin solution only exerted a very limited apoptotic effect at the tested conditions on this cell line (total apoptosis of $13.2 \pm 0.3\%$ for control nanoparticles, $7.9 \pm 0.9\%$ for plumbagin solution, similar to the $11.4 \pm 0.3\%$ apoptosis when treated with the blank nanoparticles).

In T98G cells, the apoptotic effect of Tf-bearing LPN (total apoptosis of $21.0 \pm 0.4\%$ cells) was similar to that observed with A431 cells following treatment with the same formulation but was not statistically different from that observed with control nanoparticles or drug solution (total apoptosis respectively of $17.6 \pm 1.5\%$ and $17.1 \pm 1.5\%$).

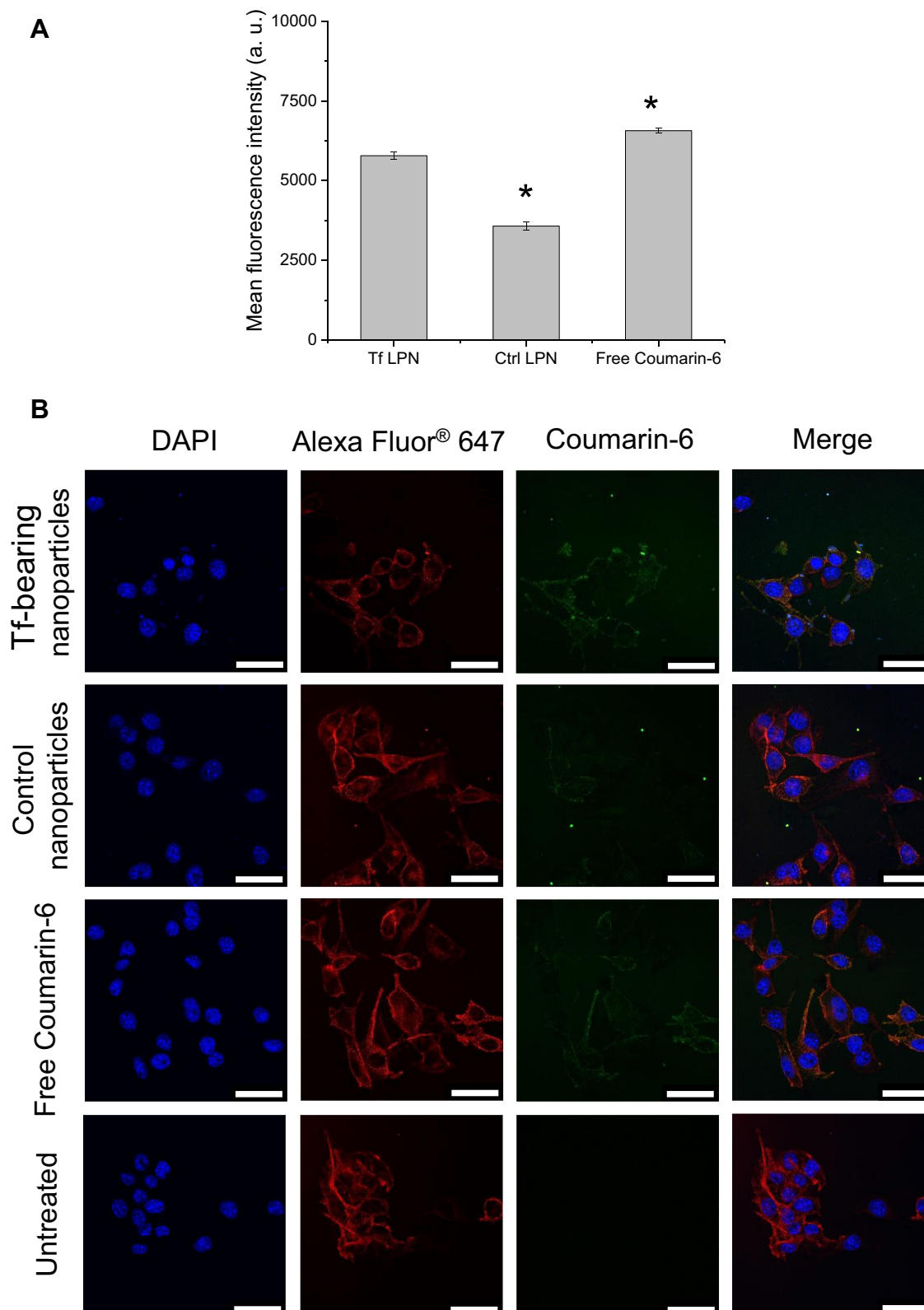


Figure 5 Uptake of coumarin-6 loaded in Tf-bearing or control lipid-polymer hybrid nanoparticles, or as solution, by B16-F10 cells: **(A)** quantitative analysis of the mean fluorescence intensity of coumarin-6 in the cells, by flow cytometry (n=9) (* $p < 0.05$ vs Tf-bearing lipid-polymer hybrid nanoparticles), **(B)** qualitative analysis by confocal microscopy (magnification: 40x).

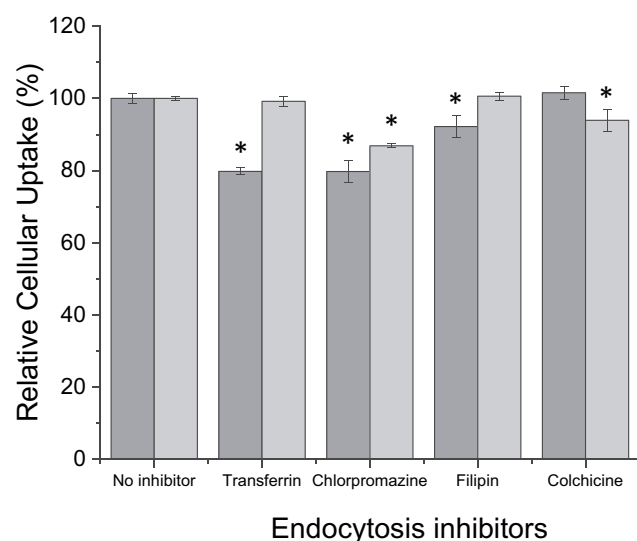


Figure 6 Relative cellular uptake of coumarin-6 loaded in Tf-bearing lipid-polymer hybrid nanoparticles (dark grey) or control lipid-polymer hybrid nanoparticles (light grey), in the presence of endocytosis inhibitors, in B16-F10 cells (n = 3) (*p<0.05 vs No inhibitor).

In vivo Tumoricidal Activity

The intravenous injection of plumbagin entrapped in Tf-bearing LPN led to an overall reduced B16-F10 tumor growth. This effect, which occurred within 24 h of the treatment, was maintained for the whole duration of the experiment. From Day 6, some of the animals bearing growing tumors had to be euthanized due to their subcutaneous tumors reaching the maximum allowed size by our Project Licence. By contrast, tumors treated with control LPN, plumbagin solution or blank nanoparticles or left untreated had a growth rate similar to that of untreated tumors, and all the animals treated with these formulations had to be euthanized after 6 days (Figure 8A). No significant variations of animal body weight or apparent signs of

animal distress were observed during the entire experiment, thus demonstrating the good tolerability of all the treatments by the animals (Figure 8B).

On the last day of the experiment, 40% of tumors treated with Tf-bearing LPN entrapping plumbagin completely disappeared, while another 10% of tumors showed a partial regression and 20% were stable (Figure 8C). By contrast, all the tumors treated with control LPN, plumbagin solution, blank nanoparticles or left untreated, were growing.

The enhanced therapeutic efficacy resulting from the treatment with Tf-bearing LPN loading plumbagin led to an extended animal survival by 26 days compared to untreated tumors (Figure 8D). Treatment with both control nanoparticles and plumbagin solution only extended mice survival by 2 days compared with untreated animals, thus emphasizing the crucial need of a tumor-targeted delivery system for the intravenous delivery of plumbagin to the tumors.

Discussion

The possibility of using plumbagin for the treatment of cancer is currently hampered by the inability of this drug to reach tumors at a therapeutic concentration, in a specific way, following intravenous injection, therefore resulting from rapid elimination. To overcome this issue, we hypothesize that the entrapment of plumbagin in a tumor-targeted delivery system would enhance its specific delivery to cancer cells and enhance its therapeutic efficacy, while reducing the secondary effects of the drug to normal tissues.

In this study, plumbagin was entrapped in novel transferrin-bearing lipid-polymer hybrid nanoparticles. PLGA-COOH, a hydrophobic and biodegradable polymer, was

Table 1 Anti-Proliferative Efficacy of Plumbagin Loaded in Tf-Bearing LPN, Control LPN or in Solution, in B16-F10, A431 and T98G Cells (Results Expressed as IC₅₀ ± SEM) (n=15)

Cell Lines	IC ₅₀ (µg/mL) (Mean ± S.E.M.)			
	Tf-LPN	Ctrl LPN	Plumbagin Solution	Blank LPN
B16-F10	0.16 ± 0.02	0.32 ± 0.01	0.51 ± 0.02	n.d.
A431	0.63 ± 0.03	1.61 ± 0.28	1.78 ± 0.20	n.d.
T98G	2.03 ± 0.15	2.40 ± 0.49	6.19 ± 0.20	n.d.

Abbreviations: ANOVA, one-way analysis of variance; DAPI, 4',6-diamidino-2-phenylindole; DMEM, Dulbecco's Modified Eagle Medium; DSPE-PEG2K-MAL, 1,2-distearoyl-sn-glycero-3-phosphoethanolamine-N-[maleimide (polyethylene glycol)-2000]; EE, entrapment efficiency; EPR, enhanced permeability and retention; FBS, fetal bovine serum; FITC, fluorescein isothiocyanate; HPC, hydrogenated phosphatidylcholine; LPN, lipid-polymer hybrid nanoparticles; MAPK, mitogen-activated protein kinase; mTOR, mammalian target of rapamycin; MTT, 3-(4,5-dimethylthiazol-2-yl)-2,5-diphenyltetrazolium bromide; NF-κB, nuclear factor-κB; PBS, phosphate buffer saline; PEG, polyethylene glycol; PI, propidium iodide; PI3K, phosphoinositide 3-kinase; PKB/AKT, protein kinase B/Akt; PLGA, poly(lactic-co-glycolic acid); PLGA-COOH, acid-terminated poly(lactide-co-glycolide); RPMI-1640, Roswell Park Memorial Institute 1640; RECIST, Response Evaluation Criteria in Solid Tumors; S.E.M, standard error of the mean; STAT3, signal transducer and activator of transcription 3; TEM, transmission electron microscopy; Tf, transferrin.

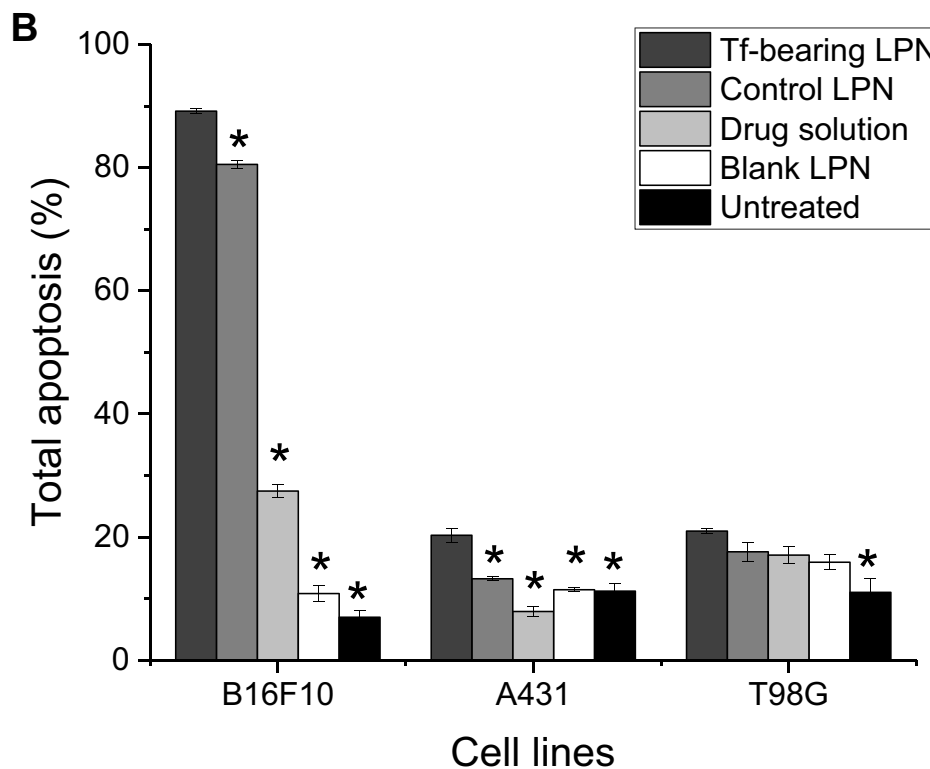
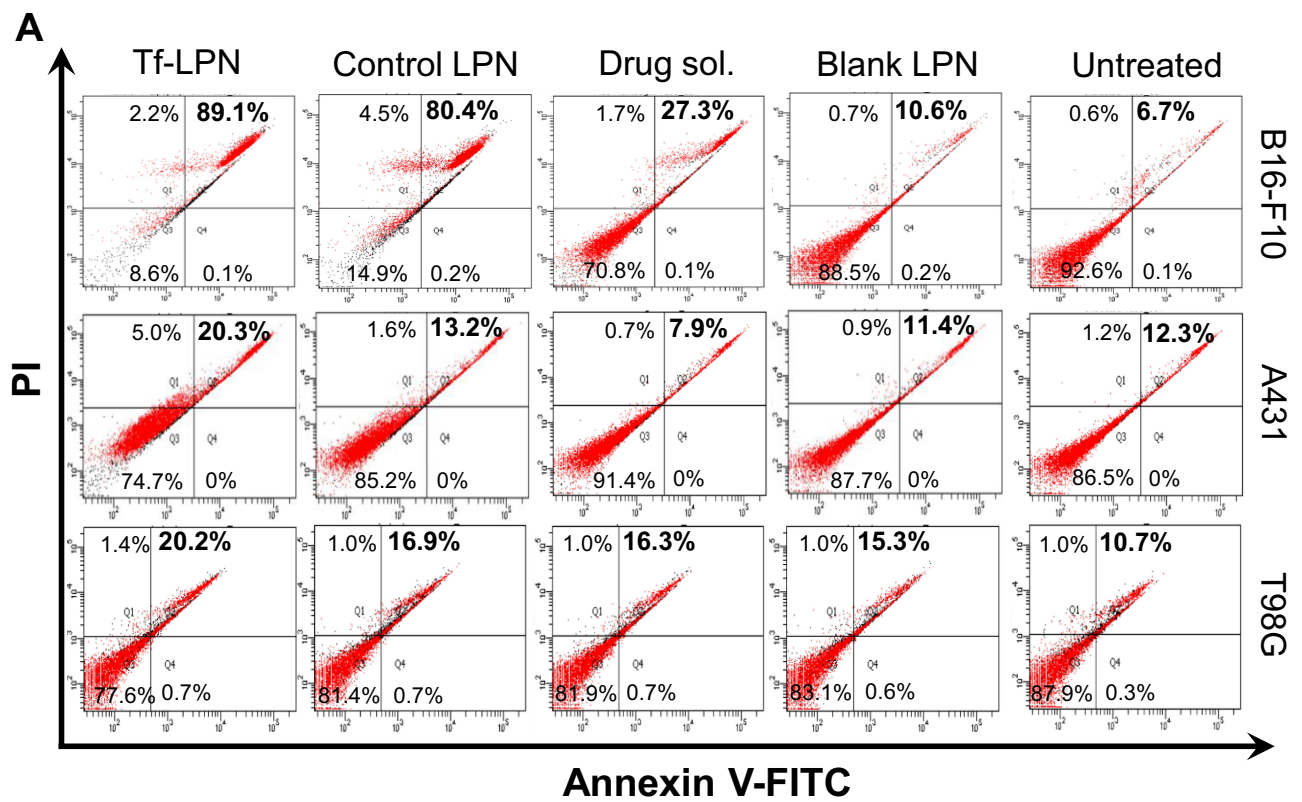


Figure 7 Apoptosis induction of B16-F10, A431 and T98G cells following treatment with plumbagin (1 $\mu\text{g/mL}$, corresponding to 5 μM) loaded in Tf-bearing or control lipid-polymer hybrid nanoparticles, or in solution. **(A)** Flow cytometric plots showing the percentage of specific cell populations in live, early apoptosis, late apoptosis and necrosis. **(B)** Percentage of total apoptotic cells (n = 3) (* $P < 0.05$ vs Tf-bearing lipid-polymer hybrid nanoparticles).

International Journal of Nanomedicine downloaded from <https://www.dovepress.com/> by 80.225.165.253 on 08-Apr-2021
For personal use only.

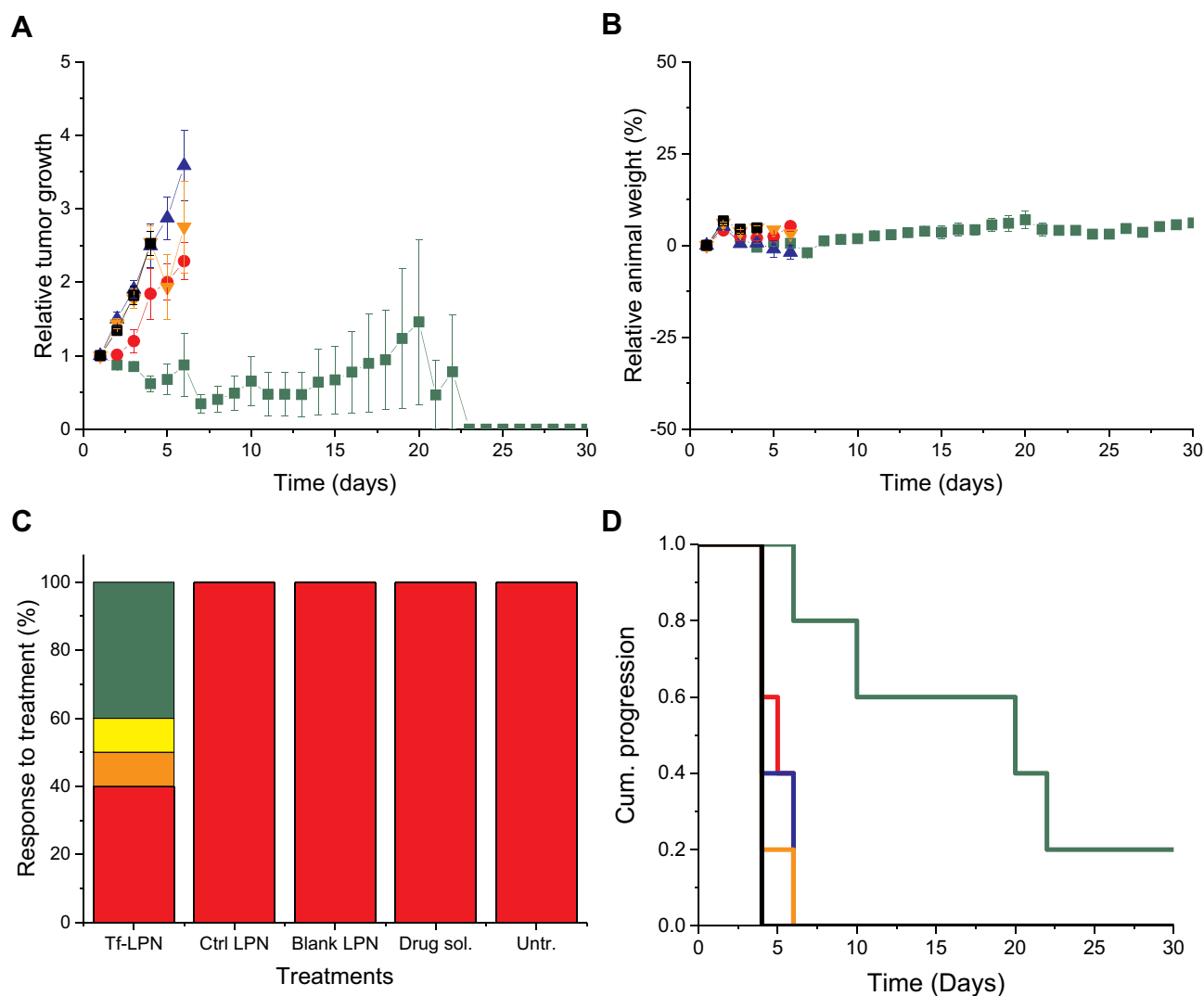


Figure 8 (A) Tumor growth studies in a B16-F10 murine model following systemic injection of transferrin-bearing lipid-polymer hybrid nanoparticles loading plumbagin (2 mg/kg of body weight/injection) (■, dark green), control lipid-polymer hybrid nanoparticles entrapping plumbagin (●, red), blank lipid-polymer hybrid nanoparticles (▲, blue), plumbagin solution (▼, orange), untreated tumors (■, black) (relative tumor volume rel. $Volt_x = Volt_x/Volt_0$) (n=10). (B) Variations of the body weight of the mice during the treatment (Color coding as in (A)). (C) Overall tumor response to treatments at the end of the study (green: complete response, yellow: partial response, orange: stable response and red: progressive response). (D) Time to disease progression. The Y-axis indicates the proportion of surviving mice over time. Animals were removed from the study once their tumor size reached 10 mm diameter in any direction. (Color coding as in (A)).

used to form the polymeric core of the hybrid nanoparticles which entrapped plumbagin, surrounded by a lipid monolayer consisting of hydrogenated phosphatidylcholine and DSPE-PEG2K-MAL that provided a stealth effect and facilitated surface modification. The LPN were successfully prepared by one-step nanoprecipitation, where the PLGA polymer in water-miscible organic solvent was mixed with the aqueous lipid dispersion to allow self-assembling. This method was more efficient, required less time and less energy than the two-step method, where lipid vesicles and polymeric nanoparticles were separately prepared before being mixed or ultrasonicated, and then homogenized.²⁸ We chose to use PLGA-COOH

for this study instead of PLGA with an ester end group, as the presence of one or two charged end groups per polymer allows a size reduction of the polymer-based nanoparticles.²⁹

The optimal formulation of LPN was found at low lipid to polymer weight ratios (10–20%), which can be explained by the fact that the entire surface of the PLGA-COOH polymer core was covered by the lipids used at these ratios.¹⁷ At high lipid to polymer weight ratios, the excess HPC and DSPE-PEG2K-MAL lipids can spontaneously form liposomes, thus resulting in an increase of the overall measured hydrodynamic size of LPN and a decrease of their zeta potential value. In addition, when

maintaining the lipid to polymer weight ratio at 20%, the increase of DSPE-PEG2K-MAL (40–50 mol%) had an impact on both the size and zeta potential of the delivery systems. This might be due to the particular conformations of PEG chains at different grafting densities.^{30,31} At low density (10–30 mol%), the PEG chains formed a mushroom configuration which has a limited impact on particle size and zeta potential. However, at high density, PEG chains tend to stretch and form a brush structure, leading to an increase in the size and zeta potential of the particles.

The conjugation of Tf to the LPN was achieved by using the thiol–maleimide “click” reaction, a widely used thiol-based bioconjugation technique for conjugating antibodies, proteins or peptides to delivery systems due to its compatibility with aqueous condition, rapid reaction (without heat or catalysts) and high selectivity.³²

Entrapment efficiency is a very important parameter to take into account in the design of drug delivery systems. In our study, plumbagin was highly loaded in both targeted and control LPN. Plumbagin has previously been reported to be entrapped in various delivery systems, such as niosomes, polymeric nanoparticles, micelles and PEGylated liposomes, with a percentage entrapment efficiency varying from 38% to 98%.^{12,13,16,33,34} We could not find any publications reporting the entrapment efficiency of plumbagin entrapped in LPN to compare with our results.

Tf-bearing LPN displayed sizes below the cut-off size for extravasation across tumor vasculature,³⁵ enabling them to efficiently deliver the drug to the tumors. They were spherical, which facilitates their uptake by cancer cells compared to other morphologies, such as ellipsoid and worm-like.^{36,37} The size of the LPN obtained from the TEM images was found to be smaller than that observed with photon correlation spectroscopy, as TEM imaging technique involves drying of the samples before measurement, unlike hydrodynamic size measurement through photon correlation spectroscopy using a Zetasizer.

They were bearing negative surface charges that were higher than that observed on the surface of control LPN. This was most likely due to the presence of the positively charged amino acids of Tf (zeta potential of -25.0 ± 3.6 mV) and ferrous iron (Fe^{2+}) in the protein.³⁸ These negative charges, together with the PEGylation of the LPN, would prevent the opsonization of the nanoparticles by serum proteins, therefore avoiding a rapid clearance by the mononuclear phagocytic system and prolonging their blood circulation time.^{39,40} In addition, the Tf-bearing

LPN can be considered as highly stable colloidal systems as their zeta potential value is lower than -30 mV.⁴¹ Furthermore, the changes in size and drug leakage of Tf-bearing and control LPN were low during 4 weeks of storage at 4°C in PBS (data not shown). Tf-bearing LPN, therefore, have the required physicochemical characteristics for being efficacious delivery systems for plumbagin.

The LPN showed a sustained release profile of plumbagin following an initial burst effect corresponding to the release of plumbagin adsorbed on the lipid surface or entrapped in the outer layer of polymer core.⁴² The subsequent sustained release of plumbagin may occur by diffusion of the drug entrapped in the polymeric core through water-filled pores, which is the most common mechanism of release reported in polymer-based nanoparticles.⁴³ In addition, Tf-bearing LPN showed a slower release of plumbagin compared with control LPN, probably because the conjugated Tf prevented the drug to freely diffuse out of the polymer core.

In vitro, the cellular uptake studies showed that the grafting of Tf to LPN significantly increased the uptake of the drug compared with control LPN and solution on the three cancer cell lines. Similar results were obtained when replacing plumbagin with the lipophilic fluorescent drug model coumarin-6. These results were in accordance with previously published data by Guo and colleagues, who showed that the use of Tf as a targeting ligand on lipid-coated PLGA nanoparticles entrapping doxorubicin improved the cellular uptake of doxorubicin by 2.8-fold compared with non-targeted nanoparticles on A549 cells.⁴⁴ This outcome was also reported by Zheng and colleagues, who showed that Tf-conjugated lipid-coated PLGA nanoparticles entrapping calcein were more efficiently taken up by SKBR-3 breast cancer cells than with the non-targeted formulation.⁴⁵

The uptake of Tf-conjugated LPN was partially inhibited by free Tf, chlorpromazine and filipin, while non-targeted LPN has its cellular uptake partially blocked by chlorpromazine and colchicine. Pre-treatment of B16-F10 cells with Tf resulted in competition between Tf-bearing LPN and Tf, suggesting that the internalization of Tf-bearing LPN is partly due to Tf receptors-mediated endocytosis. This outcome is in agreement with previous results published by Zheng and colleagues, who revealed that the cellular uptake of Tf-bearing, lipid-coated PLGA nanoparticles carrying an aromatase inhibitor was reduced by the excess free Tf in the culture medium.⁴⁵ Both chlorpromazine and filipin are pinocytosis inhibitors: chlorpromazine inhibits clathrin-mediated

endocytosis, which is a major pathway for internalization of various nanomedicines,⁴⁶ whereas filipin has been reported to block the caveolae-mediated process, a clathrin-independent endocytosis.⁴⁷ Colchicine has previously been shown to inhibit micropinocytosis, a non-specific process to internalize particles and fluids.⁴⁸ These results, therefore, confirm the involvement of clathrin-mediated endocytosis, a requisite for Tf receptor-mediated endocytosis, and caveolae-mediated endocytosis in the internalization of Tf-bearing LPN.

The conjugation of Tf to LPN led to an increase of the anti-proliferative efficacy of plumbagin-loaded LPN in all the three cancer cell lines. This might be due to the enhanced cellular uptake when treated with plumbagin formulated as Tf-conjugated LPN. The entrapment of plumbagin in various delivery systems has previously been reported to improve its therapeutic efficacy. For instance, micelles entrapping plumbagin improved its anti-proliferative efficacy by 2.1-fold compared with drug solution on MCF-7 cells.³⁴ In another study, Pawar and colleagues have demonstrated that loading plumbagin into folic acid-bearing D- α -tocopheryl PEG 1000 succinate nanomicelles was able to improve its anti-proliferative activity on MCF-7 cells, respectively by 2.4-fold and 4.1-fold in comparison with unconjugated formulation and drug solution,¹² in line with our results.

The loading of plumbagin in Tf-conjugated LPN also increased apoptosis in B16-F10 and A431 cell lines, unlike drug solution. This effect, more pronounced on B16-F10 than on A431 cells, was probably the consequence of an increased sensitivity of B16-F10 cells toward plumbagin-mediated apoptosis. Our results correlated well with previous reports by Duraipandy and colleagues, who demonstrated that the treatment of A431 cells with plumbagin loaded in silver nanocages resulted in the apoptosis of the cells, while plumbagin solution did not show any effect.⁴⁹ In another work, silver nanoparticles entrapping plumbagin was shown to induce apoptosis in HeLa cells, unlike plumbagin solution.⁵⁰ However, in T98G cells, Tf-bearing LPN entrapping plumbagin did not cause apoptosis at the tested experimental conditions. T98G cells, known to be highly resistant to alkylating agents such as temozolomide, the frontline treatment for glioblastoma multiforme,⁵¹ might also resist the alkylating properties of plumbagin.⁵²

In vivo, we demonstrated that the systemic injection of plumbagin loaded in Tf-conjugated LPN resulted in complete tumor eradication for 40% of B16-F10 tumors and tumor regression for 10% of the tumors. To our knowledge, this is the first time that intravenously administered targeted plumbagin was shown to result in regression of tumors in mice, and even to complete tumor disappearance in some instances over 30 days. Previous studies have demonstrated that plumbagin loaded in various delivery systems was able to slow down the growth of tumors, but without tumor regression or disappearance, even when using larger doses compared to the 2 mg/kg used in our study. For example, the intravenous administration of plumbagin loaded in temperature-sensitive liposomes (6 mg/kg with localized hyperthermia treatment at 43°C)¹⁴ or in PEGylated liposomes (2 mg/kg)¹³ led to a slowdown of the growth of B16F1 melanoma tumors, compared with that observed with the drug solution. Similarly, the intramuscular injection of plumbagin loaded in chitosan-based microspheres to C57BL/6J mice bearing B16F1 tumors significantly increased tumor inhibition and animals' life-span by 30% compared to free plumbagin.⁵³ In another study, the subcutaneous administration of plumbagin loaded in PLGA microspheres (10 mg/kg) to BALB/C mice led to a decrease in tumor growth of sarcoma-180 tumors compared with that obtained when treated with plumbagin solution.¹⁵ In addition, we previously demonstrated that the intravenous injection of transferrin-conjugated liposomes loading plumbagin resulted in tumor suppression for 10% of B16-F10 tumors and tumor regression for another 10% of the tumors, but these effects lasted only for a limited duration of 10 days.⁵⁴ Similarly, we also demonstrated that transferrin-bearing PLGA-PEG nanoparticles led to the complete tumor eradication for only 10% of B16-F10 tumors and regression of 30% of the tumors.⁵⁵ The strong anti-tumor effect of Tf-bearing lipid-polymer hybrid nanoparticles over the Tf-bearing liposomes may be explained as follows: 1) the lipid layer enhances the affinity of the delivery system to the lipid cell membrane, and thus increases the delivery of plumbagin to the tumors, 2) the polymeric core of the LPN provides a good stability in the blood following intravenous administration compared to liposomes, 3) the unique structure of the LPN further delayed the release of the drug compared to that observed with the liposome formulation, thereby prolonging the circulation half-life and increasing the accumulation of the drug in tumors.

The most striking effect of the tumor-targeted lipid-polymer hybrid nanoparticles was the induction of the

regression of the tumors within one day after treatment and the complete disappearance of the tumors for some animals within 10 days of treatment. There may be scope to further enhance the in vivo efficacy of these very safe delivery systems by increasing the dose, the frequency and the overall duration of the treatment, hopefully leading to a further improved therapeutic effect.

Conclusion

We have demonstrated for the first time that novel Tf-conjugated lipid-polymer hybrid nanoparticles loading plumbagin and administered intravenously resulted in a complete disappearance of 40% of B16-F10 melanoma tumors and regression of 10% of the tumors without any signs of animal distress. In contrast, all the tumors treated with control nanoparticles and plumbagin solution, or left untreated, were growing. This study provides a proof of principle that the loading of plumbagin in a tumor-targeted delivery system is a highly promising strategy for cancer treatment which should be further investigated to optimize its potential.

Acknowledgments

This work was financially supported by a Thammasat University Scholarship to I.S. [scholarship number TU_9708]. S.S. is funded by a research grant from The Dunhill Medical Trust [grant number R463/0216]. P.L. is funded by a grant from Worldwide Cancer Research [grant number 16-1303].

Disclosure

The authors report no conflicts of interest in this work.

References

1. Padhye S, Dandawate P, Yusufi M, et al. Perspectives on medicinal properties of plumbagin and its analogs. *Med. Res. Rev.* 2012;32(6):1131–1158. doi:10.1002/med.20235
2. Ahmad A, Banerjee S, Wang Z, et al. Plumbagin-induced apoptosis of human breast cancer cells is mediated by inactivation of NF-kappaB and Bcl-2. *J Cell Biochem.* 2008;105(6):1461–1471. doi:10.1002/jcb.21966
3. Thasni KA, Rakesh S, Rojini G, et al. Estrogen-dependent cell signaling and apoptosis in BRCA1-blocked BG1 ovarian cancer cells in response to plumbagin and other chemotherapeutic agents. *Ann Oncol.* 2008;19(4):696–705. doi:10.1093/annonc/mdm557
4. Hsu YL, Cho CY, Kuo PL, et al. Plumbagin (5-hydroxy-2-methyl-1,4-naphthoquinone) induces apoptosis and cell cycle arrest in A549 cells through p53 accumulation via c-Jun NH2-terminal kinase-mediated phosphorylation at serine 15 in vitro and in vivo. *J Pharmacol Exp Ther.* 2006;318:484–494. doi:10.1124/jpet.105.098863
5. Powolny AA, Singh SV. Plumbagin-induced apoptosis in human prostate cancer cells is associated with modulation of cellular redox status and generation of reactive oxygen species. *Pharm Res.* 2008;25:2171–2180. doi:10.1007/s11095-008-9533-3
6. Wang CC, Chiang YM, Sung SC, et al. Plumbagin induces cell cycle arrest and apoptosis through reactive oxygen species/c-Jun N-terminal kinase pathways in human melanoma A375.S2 cells. *Cancer Lett.* 2008;259(1):82–98. doi:10.1016/j.canlet.2007.10.005
7. McKallip RJ, Lombard C, Sun J, et al. Plumbagin-induced apoptosis in lymphocytes is mediated through increased reactive oxygen species production, upregulation of Fas, and activation of the caspase cascade. *Toxicol Appl Pharmacol.* 2010;247:41–52. doi:10.1016/j.taap.2010.05.013
8. Lai L, Liu J, Zhai D, et al. Plumbagin inhibits tumour angiogenesis and tumour growth through the Ras signalling pathway following activation of the VEGF receptor-2. *Br J Pharmacol.* 2012;165:1084–1096. doi:10.1111/j.1476-5381.2011.01532.x
9. Yan W, Tu B, Liu YY, et al. Suppressive Effects of plumbagin on invasion and migration of breast cancer cells via the inhibition of STAT3 signaling and down-regulation of inflammatory cytokine expressions. *Bone Res.* 2013;1:362–370. doi:10.4248/BR201304007
10. Hafeez BB, Fischer JW, Singh A, et al. Plumbagin inhibits prostate carcinogenesis in intact and castrated PTEN knockout mice via targeting PKC ϵ , Stat3 and epithelial to mesenchymal transition markers. *Cancer Prev Res.* 2015;8:375–386. doi:10.1158/1940-6207.CAPR-14-0231
11. Pan ST, Qin Y, Zhou ZW, et al. Plumbagin induces G(2)/M arrest, apoptosis, and autophagy via p38 MAPK- and PI3K/Akt/mTOR-mediated pathways in human tongue squamous cell carcinoma cells. *Drug Des Devel Ther.* 2015;9:1601–1626. doi:10.2147/DDDT.S76057
12. Pawar A, Patel R, Arulmozhi S, et al. d- α -Tocopheryl polyethylene glycol 1000 succinate conjugated folic acid nanomicelles: towards enhanced bioavailability, stability, safety, prolonged drug release and synergized anticancer effect of plumbagin. *RSC Adv.* 2016;6(81):78106–78121. doi:10.1039/C6RA12714B
13. Kumar MR, Aithal BK, Udupa N, et al. Formulation of plumbagin loaded long circulating pegylated liposomes: in vivo evaluation in C57BL/6J mice bearing B16F1 melanoma. *Drug Deliv.* 2011;18:511–522. doi:10.3109/10717544.2011.595840
14. Tiwari SB, Pai RM, Udupa N. Temperature sensitive liposomes of plumbagin: characterization and in vivo evaluation in mice bearing melanoma B16F1. *J Drug Target.* 2002;10:585–591. doi:10.1080/1061186021000054924
15. Singh UV, Bisht KS, Rao S, et al. Plumbagin-loaded PLGA microspheres with reduced toxicity and enhanced antitumour efficacy in mice. *Pharm Pharmacol Commun.* 1996;2:407–409.
16. Pan M, Li W, Yang J, et al. Plumbagin-loaded aptamer-targeted poly d,l-lactic-co-glycolic acid-b-polyethylene glycol nanoparticles for prostate cancer therapy. *Medicine.* 2017;96(30):e7405. doi:10.1097/MD.0000000000007405
17. Zhang L, Chan JM, Gu FX, et al. Self-assembled lipid-polymer hybrid nanoparticles: a robust drug delivery platform. *ACS Nano.* 2008;2(8):1696–1702. doi:10.1021/nn800275r
18. Daniels TR, Bernabeu E, Rodríguez JA, et al. Transferrin receptors and the targeted delivery of therapeutic agents against cancer. *Biochim Biophys Acta.* 2012;1820:291–317. doi:10.1016/j.bbagen.2011.07.016
19. Dufès C, Al Robaian M, Somani S. Transferrin and the transferrin receptor for the targeted delivery of therapeutic agents to the brain and cancer cells. *Ther Deliv.* 2013;4:629–640. doi:10.4155/tde.13.21
20. Fu JY, Blatchford DR, Tetley L, et al. Tumor regression after systemic administration of tocotrienol entrapped in tumor-targeted vesicles. *J Control Release.* 2009;140(2):95–99. doi:10.1016/j.jconrel.2009.08.017

21. Fu JY, Zhang W, Blatchford DR, et al. Novel tocotrienol-entrapping vesicles can eradicate solid tumors after intravenous administration. *J Control Release*. 2011;154(1):20–26. doi:10.1016/j.jconrel.2011.04.015
22. Lemarié F, Chang CW, Blatchford DR, et al. Anti-tumor activity of the tea polyphenol epigallocatechin gallate encapsulated in targeted vesicles after intravenous administration. *Nanomedicine*. 2013;8:181–192. doi:10.2217/nmm.12.83
23. Karim R, Somani S, Al Robaian M, et al. Tumor regression after intravenous administration of targeted vesicles entrapping the vitamin E α -tocotrienol. *J Control Release*. 2017;246:79–87. doi:10.1016/j.jconrel.2016.12.014
24. Maeda H, Wu J, Sawa T, et al. Tumor vascular permeability and the EPR effect in macromolecular therapeutics: a review. *J Control Release*. 2000;65(1–2):271–284. doi:10.1016/S0168-3659(99)00248-5
25. Lowry OH, Rosebrough NJ, Farr AL, et al. Protein measurement with the Folin phenol reagent. *J Biol Chem*. 1951;193(1):265–275. doi:10.1016/S0021-9258(19)52451-6
26. Dufès C, Schätzlein AG, Tetley L, et al. Niosomes and polymeric chitosan based vesicles bearing transferrin and glucose ligands for drug targeting. *Pharm Res*. 2000;17:1250–1258. doi:10.1023/A:1026422915326
27. Eisenauer EA, Therasse P, Bogaerts J, et al. New response evaluation criteria in solid tumours: revised RECIST guideline (version 1.1). *Eur J Cancer*. 2009;45:228–247. doi:10.1016/j.ejca.2008.10.026
28. Hadinoto K, Sundaresan A, Cheow WS. Lipid-polymer hybrid nanoparticles as a new generation therapeutic delivery platform: a review. *Eur J Pharm Biopharm*. 2013;85:427–443. doi:10.1016/j.ejpb.2013.07.002
29. Reisch A, Runser A, Arntz Y, Mèly Y, Klymchenko AS. Charge-controlled nanoprecipitation as a modular approach to ultrasmall polymer nanocarriers: making bright and stable nanoparticles. *ACS Nano*. 2015;9(5):5104–5116. doi:10.1021/acsnano.5b00214
30. Zhan X, Tran KK, Shen H. Effect of the poly(ethylene glycol) (PEG) density on the access and uptake of particles by antigen-presenting cells (APCs) after subcutaneous administration. *Mol Pharm*. 2012;9:3442–3451. doi:10.1021/mp300190g
31. Zhang S, Tang C, Yin C. Effects of poly(ethylene glycol) grafting density on the tumor targeting efficacy of nanoparticles with ligand modification. *Drug Deliv*. 2015;22(2):182–190. doi:10.3109/10717544.2013.854849
32. Stenzel MH. Bioconjugation using thiols: old chemistry rediscovered to connect polymers with nature's building blocks. *ACS Macro Lett*. 2013;2(1):14–18. doi:10.1021/mz3005814
33. Naresh RAR, Udupa N, Devi PU. Niosomal plumbagin with reduced toxicity and improved anticancer activity in BALB/C mice. *J Pharm Pharmacol*. 1996;48:1128–1132. doi:10.1111/j.2042-7158.1996.tb03907.x
34. Bothiraja C, Kapare HS, Pawar AP, et al. Development of plumbagin-loaded phospholipid-Tween® 80 mixed micelles: formulation, optimization, effect on breast cancer cells and human blood/serum compatibility testing. *Ther Deliv*. 2013;4:1247–1259. doi:10.4155/tde.13.92
35. Yuan F, Dellian M, Fukumura D, et al. Vascular permeability in a human tumor xenograft: molecular size dependence and cutoff size. *Cancer Res*. 1995;55:3752–3756.
36. Herd H, Daum N, Jones AT, et al. Nanoparticle Geometry and Surface Orientation Influences Mode of Cellular Uptake. *ACS Nano*. 2013;7(3):1–21. doi:10.1021/nn304439f
37. Toy R, Peiris PM, Ghaghada KB, et al. Shaping cancer nanomedicine: the effect of particle shape on the in vivo journey of nanoparticles. *Nanomedicine*. 2014;9:121–134. doi:10.2217/nmm.13.191
38. Gan CW, Feng SS. Transferrin-conjugated nanoparticles of Poly(lactide)-d- α -Tocopheryl polyethylene glycol succinate diblock copolymer for targeted drug delivery across the blood-brain barrier. *Biomaterials*. 2010;31:7748–7757. doi:10.1016/j.biomaterials.2010.06.053
39. Ernsting MJ, Murakami M, Roy A, et al. Factors Controlling the Pharmacokinetics, Biodistribution and Intratumoral Penetration of Nanoparticles. *J Control Release*. 2013;172:782–794. doi:10.1016/j.jconrel.2013.09.013
40. Blanco E, Shen H, Ferrari M. Principles of nanoparticle design for overcoming biological barriers to drug delivery. *Nat Biotechnol*. 2015;33:941–951. doi:10.1038/nbt.3330
41. Bhattacharjee S. DLS and zeta potential – what they are and what they are not? *J Control Release*. 2016;235:337–351. doi:10.1016/j.jconrel.2016.06.017
42. Garg NK, Tyagi RK, Sharma G, et al. Functionalized lipid-polymer hybrid nanoparticles mediated codelivery of methotrexate and aceclofenac: a synergistic effect in breast cancer with improved pharmacokinetics attributes. *Mol Pharm*. 2017;14:1883–1897. doi:10.1021/acs.molpharmaceut.6b01148
43. Fredenberg S, Wahlgren M, Reslow M, et al. The mechanisms of drug release in poly(lactic-co-glycolic acid)-based drug delivery systems—a review. *Int J Pharm*. 2011;415(1–2):34–52. doi:10.1016/j.ijpharm.2011.05.049
44. Guo L, Zhang H, Wang F, et al. Targeted multidrug-resistance reversal in tumor based on PEG-PLL-PLGA polymer nano drug delivery system. *Int J Nanomedicine*. 2015;10:4535–4547. doi:10.2147/IJN.S85587
45. Zheng Y, Yu B, Weecharangsan W, et al. Transferrin-conjugated lipid-coated PLGA nanoparticles for targeted delivery of aromatase inhibitor 7 α -APTADD to breast cancer cells. *Int J Pharm*. 2010;390:234–241. doi:10.1016/j.ijpharm.2010.02.008
46. Chen F, Zhu L, Zhang Y, et al. Clathrin-mediated endocytosis is a candidate entry sorting mechanism for Bombyx mori cyovirus. *Sci Rep*. 2018;8:7268. doi:10.1038/s41598-018-25677-1
47. Gao H, Yang Z, Zhang S, et al. Ligand modified nanoparticles increases cell uptake, alters endocytosis and elevates glioma distribution and internalization. *Sci Rep*. 2013;3:2534. doi:10.1038/srep02534
48. Oh N, Park JH. Endocytosis and exocytosis of nanoparticles in mammalian cells. *Int J Nanomedicine*. 2014;9(Suppl 1):51–63. doi:10.2147/IJN.S26592
49. Duraipandy N, Lakra R, Kunnakkam Vinjimur S, et al. Caging of plumbagin on silver nanoparticles imparts selectivity and sensitivity to plumbagin for targeted cancer cell apoptosis. *Metallomics*. 2014;6(11):2025–2033. doi:10.1039/C4MT00165F
50. Appadurai P, Rathinasamy K. Plumbagin-silver nanoparticle formulations enhance the cellular uptake of plumbagin and its antiproliferative activities. *IET Nanobiotechnol*. 2015;9(5):264–272. doi:10.1049/iet-nbt.2015.0008
51. Kriel J, Müller NK, Maarman G, et al. Coordinated autophagy modulation overcomes glioblastoma chemoresistance through disruption of mitochondrial bioenergetics. *Sci Rep*. 2018;8:10348. doi:10.1038/s41598-018-28590-9
52. Klotz LO, Hou X, Jacob C. 1,4-naphthoquinones: from oxidative damage to cellular and inter-cellular signaling. *Molecules*. 2014;19:14902–14918. doi:10.3390/molecules190914902
53. Rayabandla SKM, Aithal K, Anandam A, et al. Preparation, in vitro characterization, pharmacokinetic, and pharmacodynamic evaluation of chitosan-based plumbagin microspheres in mice bearing B16F1 melanoma. *Drug Deliv*. 2010;17:103–113. doi:10.3109/10717540903548447
54. Sakpakdeeroen I, Somani S, Laskar P, et al. Transferrin-targeted liposomes entrapping plumbagin for cancer therapy. *JOIN*. 2019;4:54–71.
55. Sakpakdeeroen I, Somani S, Laskar P, et al. Anti-Tumor Activity of Intravenously Administered Plumbagin Entrapped in Targeted Nanoparticles. *J Biomed Nanotechnol*. 2020;16(1):85–100. doi:10.1166/jbn.2020.2874

International Journal of Nanomedicine

Dovepress

Publish your work in this journal

The International Journal of Nanomedicine is an international, peer-reviewed journal focusing on the application of nanotechnology in diagnostics, therapeutics, and drug delivery systems throughout the biomedical field. This journal is indexed on PubMed Central, MedLine, CAS, SciSearch[®], Current Contents[®]/Clinical Medicine,

Journal Citation Reports/Science Edition, EMBase, Scopus and the Elsevier Bibliographic databases. The manuscript management system is completely online and includes a very quick and fair peer-review system, which is all easy to use. Visit <http://www.dovepress.com/testimonials.php> to read real quotes from published authors.

Submit your manuscript here: <https://www.dovepress.com/international-journal-of-nanomedicine-journal>